

Original Article

Enhanced intracellular delivery and controlled drug release of magnetic PLGA nanoparticles modified with transferrin

Yan-na CUI^{1,2,3}, Qing-xing XU¹, Pooya DAVOODI¹, De-ping WANG^{2,*}, Chi-Hwa WANG^{1,*}

¹Department of Chemical and Biomolecular Engineering, National University of Singapore, Singapore 117585, Singapore; ²School of Materials Science and Engineering, Tongji University, Shanghai 201804, China; ³Key Laboratory of Primate Neurobiology, Institute of Neuroscience, Shanghai Institute for Biological Sciences, Chinese Academy of Sciences, Shanghai 200031, China

Abstract

Owing to the presence of multidrug resistance in tumor cells, conventional chemotherapy remains clinically intractable. To enhance the therapeutic efficacy of chemotherapeutic agents, targeting strategies based on magnetic polymeric nanoparticles modified with targeting ligands have gained significant attention in cancer therapy. In this study, we synthesized transferrin (Tf)-modified poly(*D,L*-lactic-co-glycolic acid) nanoparticles (PLGA NPs) loaded with paclitaxel (PTX) and superparamagnetic nanoparticle (MNP) using a solid-in-oil-in-water solvent evaporation method, followed by Tf adsorption on the surface of NPs. The Tf-modified magnetic PLGA NPs were characterized in terms of particle morphology and size, magnetic properties, encapsulation efficiency and drug release. Furthermore, the cytotoxicity and cellular uptake of the drug-loaded magnetic PLGA NPs were evaluated in both MCF-7 breast cancer and U-87 glioma cells *in vitro*. We found that Tf-modified PTX-MNP-PLGA NPs showed the highest cytotoxicity effect and cellular uptake efficiency under Tf receptor mediation in both MCF-7 and U-87 cells compared to unmodified PLGA NPs and free PTX. The cellular uptake efficiency of Tf-modified magnetic PLGA NPs appeared to be facilitated by the applied magnetic field, but the difference did not reach statistical significance. This study illustrates that this proposed formulation can be used as one new alternative treatment for patients bearing inaccessible tumors.

Keywords: magnetic nanoparticle; transferrin receptors; paclitaxel; targeted drug delivery; MCF-7 breast cancer; U-87 glioma cells; nanomedicine

Acta Pharmacologica Sinica (2017) 38: 943–953; doi: 10.1038/aps.2017.45; published online 22 May 2017

Introduction

With the advent of novel chemotherapeutic drugs, chemotherapy has been widely used to inhibit tumor growth and metastasis in cancer patients^[1,2]. For instance, paclitaxel (PTX) is a mitotic inhibitor and is used to treat a variety of solid tumors involving the brain, breast, lung, bladder, and ovary^[3–7]. However, the potential of these novel drugs is often limited by the severe toxicity imposed on normal tissues of the body resulting from their systemic delivery and the multidrug resistance (MDR) in tumor cells that can extrude drugs using transporter proteins^[8,9].

The use of biocompatible and biodegradable poly(*D,L*-lactic-co-glycolic acid) nanoparticles (PLGA NPs) as a drug

delivery system has been widely investigated for various biomedical applications, particularly for cancer treatment^[10]. PLGA NPs are advantageous in terms of their sustained release property, protection of the drug from degradation and well-described formulations to deliver various therapeutics with favorable drug release profiles^[11,12]. PLGA NPs are not affected by cell membrane-associated efflux transporters since the drug is well encapsulated. It is expected that these NPs could escape the efflux action of these transporters and lead to greater cellular uptake than free drug formulations. In addition, once the NPs enter cancer cells, intracellular release of the drug in a controlled manner can preserve the drug effect and improve the therapeutic efficiency.

Magnetic nanoparticle (MNP) can become magnetic in a magnetic field and lose this magnetism after the magnetic field is removed^[13]. Although this form of the superparamagnetic property has been extensively exploited in bio-imaging, chemotherapeutic drugs can also be directed toward a specific tis-

*To whom correspondence should be addressed.

E-mail chewch@nus.edu.sg (Chi-Hwa WANG);

wdpshk@tongji.edu.cn (De-ping WANG)

Received 2016-11-18 Accepted 2017-04-05

sue by applying a magnetic field^[14, 15]. Thus, the incorporation of MNP into PLGA NPs can enhance the delivery of drugs to a target site in the body while reducing systemic toxicity and increasing drug efficacy^[16].

In addition, the conjugation of targeting moieties, such as peptides, proteins and aptamers^[17-19], to polymeric carriers could offer an effective approach to target drugs to tumor cells^[20]. Transferrin (Tf), an iron-binding plasma glycoprotein, is crucial for the cellular transport of iron mediated by cell surface Tf receptors, and such receptors have been found to be overexpressed in proliferating cancer cells compared to normal tissues. Cell surface Tf receptors can bind diferric Tf (holo-Tf) with high affinity, and Tf-modified PLGA NPs can be internalized through receptor-mediated endocytosis^[21].

The aim of this study is to explore the feasibility of drug- and MNP-loaded PLGA NPs modified with Tf to enhance cellular uptake and improve therapeutic efficiency in cancer cells. PTX was selected as the model antiproliferative drug to load into PLGA NPs. PLGA NPs were synthesized and characterized in terms of particle morphology and size, magnetic properties, encapsulation efficiency and drug release. Unlike previously developed Tf-conjugated PLGA NPs^[22-25], here, we have employed an adsorption technique for the functionalization of NPs without covalent grafting. Finally, the cytotoxicity and cellular uptake of the drug-loaded PLGA NPs were evaluated *in vitro* in MCF-7 breast cancer and U-87 glioma cells.

Materials and methods

Materials

Ammonium hydroxide (NH₃·H₂O, 28%–30%), iron (III) chloride hexahydrate (FeCl₃·6H₂O, 98%), human holo-transferrin (≥98%), sodium sulfite (Na₂SO₃, ≥98%), poly(vinyl alcohol) (PVA, M_w=30–70 kDa), dichloromethane (DCM), zinc sulfate monohydrate (ZnSO₄·H₂O), coumarin-6 (CM), hydrochloric acid (HCl), oleic acid (OA, ≥99%), acetonitrile (ACN, ≥99.5%), calcium chloride dihydrate (CaCl₂·2H₂O), potassium chloride (KCl), magnesium sulfate (MgSO₄), monobasic sodium phosphate (NaH₂PO₄), sodium chloride (NaCl), 4-(2-hydroxyethyl) piperazine-1-ethanesulfonic acid (HEPES) and D-glucose were obtained from Sigma-Aldrich Corp (St Louis, MO, USA). PLGA 50:50 (inherent viscosity=0.24–0.54 dL/g in hexafluoroisopropanol) was purchased from Lactel Absorbable Polymers (Pelham, AL, USA). The CellTiter 96[®] Non-Radioactive Cell Proliferation Assay was purchased from Promega Corp (Madison, WI, USA). Phosphate-buffered saline (PBS, pH=7.4) was purchased from Mediatech, Inc (Manassas, VA, USA). Paclitaxel (PTX) was kindly supplied by Bristol-Myers Squibb Company (New York, NY, USA) at no cost.

Preparation of oleic acid-modified magnetic nanoparticle (OA-MNP)

MNP was prepared with reference to the protocol reported in the previous work^[26]. Briefly, FeCl₃ (8 mL, 1 mol/L), Na₂SO₃ (1.5 mL, 1 mol/L) and NH₃·H₂O (5 mL, 28%–30%) solutions were added to 100 mL of deionized water and heated with stirring under nitrogen at 70–80 °C for 30 min. While heating,

0.33 mL of OA was added to modify the surface of MNP with OA before further incubating the mixture at 80 °C for 50 min. The temperature was then raised to 110 °C to evaporate excess ammonium hydroxide and water. Finally, HCl was added to precipitate the MNP. The oleic acid-modified MNP (OA-MNP) was removed from the solution using a magnet, washed repeatedly with acetone and deionized water and lyophilized to obtain the powder.

Preparation of PTX- and MNP-loaded PLGA NPs (PTX-MNP-PLGA NPs)

PTX- and MNP-loaded PLGA NPs (PTX-MNP-PLGA NPs) were prepared according to the protocol reported in previous studies^[27, 28]. Briefly, 20 mg of PTX and 100 mg of PLGA were dissolved in 1 mL of DCM. Varying amounts of OA-MNP were added to the solution, and the mixture was sonicated using a microtip probe sonicator (VC 505, Sonics & Materials, Inc, Newtown, CT, USA) at 25% amplitude for 1 min. Following that, the mixture was combined with PVA (2 mL, 2% or 4% (*w/v*) in water) and sonicated for another 1 min. After that, the mixture was dropwise added into more PVA solution (48 mL, 0.05% (*w/v*) in water) and stirred for 24 h to ensure complete evaporation of the organic solvent. The samples were washed repeatedly with deionized water and lyophilized. CM- and MNP-loaded PLGA NPs (CM-MNP-PLGA NPs) were also prepared in a similar manner by loading 0.05% (*w/w*) CM in PLGA. MNP-loaded PLGA NPs (MNP-PLGA NPs) were also synthesized in a similar manner without the addition of any drug.

Preparation of Tf-modified PTX- and MNP-loaded PLGA NPs (Tf-modified PTX-MNP-PLGA NPs)

Tf-modified PTX- and MNP-loaded PLGA NPs (Tf-modified PTX-MNP-PLGA NPs) were prepared based on a reported procedure^[25, 29, 30]. Tf solutions were first prepared in Ringer-Hepes buffer (pH=7.4, containing 1.8 mmol/L CaCl₂, 5.6 mmol/L KCl, 0.8 mmol/L MgSO₄, 0.8 mmol/L NaH₂PO₄, 116 mmol/L NaCl, 25 mmol/L HEPES and 5.5 mmol/L D-glucose) at different concentrations ranging from 0.2 to 1.0 mg/mL. Then, 30 mg of PTX-MNP-PLGA NPs was added to the above solutions, and the samples were moderately shaken at room temperature for 3 h. Lastly, the sample was ultra-filtered to remove free Tf, washed and lyophilized. Tf-modified CM-MNP-PLGA NPs were also prepared in a similar manner. The amount of Tf adsorbed on the surface of PLGA NPs was determined using a BCA Protein Assay Kit (Thermo Fisher Scientific, Inc, Rockford, IL, USA).

Characterization of PLGA NPs

The PLGA NPs were characterized by visualizing their morphology via transmission electron microscopy (TEM, Tecnai G2 F20, FEI Company, Hillsboro, OR, USA) with a resolution of 0.14 nm for lattice images and 0.25 nm for point images, measuring their hydrodynamic size via dynamic light scattering (DLS, 90Plus Particle Size Analyzer, Brookhaven Instruments Corp, Holtsville, NY, USA), analyzing their magnetic

properties via vibrating sample magnetometry (VSM, EV7, MicroSense, LLC, Lowell, MA, USA), and examining their thermal stability via thermogravimetric analysis (TGA, DTG-60H, Shimadzu Corp, Kyoto, Japan). The surface functional groups of the samples were analyzed by Fourier transform infrared spectroscopy (FTIR, Excalibur FTS 3500GX, Bio-Rad Laboratories, Inc, Cambridge, MA, USA).

Encapsulation efficiency

The encapsulation efficiency of PTX in PLGA NPs was determined by high-performance liquid chromatography (HPLC, 1200 Series, Agilent Technologies, Inc, Santa Clara, CA, USA). Briefly, 2 mg of sample was dissolved in 1 mL of DCM to extract PTX from PLGA NPs in triplicate. After solvent evaporation, the residue was re-dissolved in 1 mL of mobile phase (70:30 ACN to H₂O ratio), and the solution was filtered through a 0.2- μ m syringe filter before analysis by HPLC using a C18 column. The mobile phase was delivered at a rate of 1 mL/min. A total of 100 μ L of the sample was injected by an auto-sampler, and the column effluent was measured at 227 nm using an ultraviolet (UV) detector. The column was maintained at 25°C. PTX samples of standard concentrations were used to produce the calibration plot. The encapsulation efficiency of PTX was calculated as the percentage of the initial amount of PTX used that was entrapped in the PLGA NPs.

In vitro drug release

For each batch of PTX-MNP-PLGA NPs, approximately 10 mg of sample was suspended in 20 mL of PBS with 0.05% (*w/v*) Tween 80 in triplicate. The samples were incubated at 37°C and continuously shaken at 150 rounds per minute. The supernatant was removed at designated time points and replaced with fresh PBS to maintain constant pH and sink conditions. To determine the amount of PTX, the drug was extracted from the supernatant using DCM. After the DCM was evaporated, the residue was re-dissolved in 1 mL of mobile phase (70:30 ACN to H₂O ratio). Finally, the solution was filtered through a 0.2- μ m syringe filter before analyzing with HPLC.

Cell culture and maintenance

MCF-7 is a breast cancer cell line (ATCC Number: HTB-22TM) derived from a 69-year-old Caucasian woman. U-87 MG is a glioblastoma, astrocytoma cell line (ATCC Number: HTB-14TM) derived from the malignant glioma of a 44-year-old Caucasian man. All cells were incubated at 37°C and 5% CO₂. The medium used for cell culture was Dulbecco's modified Eagle's medium (DMEM) (Gibco, Life Technologies Corp, Carlsbad, CA, USA) supplemented with 1% penicillin-streptomycin (PS) (PAN-Biotech GmbH, Aidenbach, Germany) and 10% fetal bovine serum (FBS) (HyClone, Thermo Fisher Scientific, Inc, Logan, UT, USA).

In vitro cytotoxicity

The cytotoxic effects of Tf-modified PTX-MNP-PLGA NPs, Tf-modified PTX-MNP-PLGA NPs with free Tf, PTX-MNP-PLGA

NPs and free PTX were examined in MCF-7 and U-87 cells. Briefly, cells were cultured in 96-well plates at 5×10^3 cells per well for 24 h before treating them with different concentrations of Tf-modified PTX-MNP-PLGA NPs, Tf-modified PTX-MNP-PLGA NPs with free Tf, PTX-MNP-PLGA NPs and free PTX. For Tf-modified PTX-MNP-PLGA NPs with free Tf, free Tf was added together with the drug-loaded NPs to the cells. The cell viability was then measured 24 and 96 h after treatment using a CellTiter 96[®] Non-Radioactive Cell Proliferation Assay (Promega Corp, Madison, WI, USA). The cells were rinsed with PBS before adding 100 μ L of fresh culture medium and 15 μ L of dye solution. The plates were further incubated for 4 h. Then, 100 μ L of solubilization solution was added to the cells, and the plates were gently shaken at room temperature for 24 h. The absorbance of the sample was measured with six replicates using a spectrophotometer at 570 nm with a reference wavelength of 630 nm.

Internalization pathway of nanoparticles

Qualitative intracellular uptake study

For the qualitative study tracking the cellular uptake of drug-loaded PLGA NPs, cells were cultured in 24-well plates with glass cover slips at 5×10^4 cells per well for 24 h before they were treated with Tf-modified CM-MNP-PLGA NPs, Tf-modified CM-MNP-PLGA NPs with free Tf, CM-MNP-PLGA NPs or free CM at a concentration of 100 μ g/mL. The cells were then prepared for confocal imaging 2 and 8 h after treatment. The cells were rinsed with PBS and fixed with a 70% cold ethanol solution at room temperature for 20 min. The cells were then rinsed with PBS three times before staining with Hoechst dye (1 μ g/mL) for 45 min. Finally, the cells were again rinsed with PBS three times. The cover slips with attached cell monolayers were inverted with the cell layer face down onto microscope slides and visualized using a Fluoview FV1000 laser scanning confocal microscope (Olympus Corp, Tokyo, Japan), with the corresponding confocal images captured by Olympus Fluoview software.

Quantitative intracellular uptake study

For the quantitative study to determine the intracellular CM level from the cellular uptake of drug-loaded PLGA NPs, cells were cultured in 24-well plates at 5×10^4 cells per well for 24 h before treating them with Tf-modified CM-MNP-PLGA NPs with a magnetic field, Tf-modified CM-MNP-PLGA NPs, Tf-modified CM-MNP-PLGA NPs with free Tf, CM-MNP-PLGA NPs or free CM at a concentration of 100 μ g/mL. For Tf-modified CM-MNP-PLGA NPs with a magnetic field, the cells treated with drug-loaded PLGA NPs were subjected to 0.1 T neodymium-iron-boron permanent magnets (Master Magnetics, Inc, Castle Rock, CO, USA) placed externally under each well. Following 2 and 8 h of treatment, the cells were rinsed with PBS, lysed with 200 μ L of 0.5% (*w/w*) Triton-X 100 in 0.2 mol/L NaOH solution^[31], and shaken for 15 min. The fluorescence intensity of the sample was measured by a microplate reader at excitation and emission wavelengths of 430 and 505 nm, respectively. The fractional amount of CM within

the cells was calculated as the amount of CM within the cells (fluorescence intensity) divided by the total amount of CM (fluorescence intensity of the sample from the known NP concentration under the same conditions of cell incubation but without washing the cells with PBS).

For the quantitative study on determining the intracellular PTX level from the cellular uptake of drug-loaded PLGA NPs, cells were cultured in 24-well plates at 5×10^4 cells per well for 24 h before treating them with Tf-modified PTX-MNP-PLGA NPs with a magnetic field, Tf-modified PTX-MNP-PLGA NPs, Tf-modified PTX-MNP-PLGA NPs with free Tf, PTX-MNP-PLGA NPs or free PTX at a concentration of 100 $\mu\text{g}/\text{mL}$. Following 2 and 8 h of treatment, the medium from each well was collected. Cells were rinsed with PBS to remove surface-bound PLGA NPs or free PTX, and the PBS was also collected. The two solutions were combined, and ZnSO_4 was added to precipitate the protein. The suspension was vortexed for 5 min before adding DCM to extract PTX. The mixture was vortexed and kept at room temperature for 1 h. The DCM was evaporated before re-dissolving the drug in 1 mL of mobile phase (70:30 ACN to H_2O ratio). The solution was then filtered through a 0.2- μm syringe filter before analysis with HPLC to evaluate the amount of PTX that was not taken up by the cells (A). Cells were treated with trypsin, extracted, and centrifuged at 5000 rounds per minute for 15 min. The supernatant was removed, and ZnSO_4 was added to it. DCM was then added to extract PTX. The DCM was evaporated before re-dissolving the drug in the mobile phase. The solution was then filtered and analyzed using HPLC to evaluate the amount of PTX within the cells (B). The fractional amount of PTX within the cells (X) was calculated as the amount of PTX within the cells (B) divided by the total amount of PTX (A+B).

Results

Morphology of MNP-PLGA NPs

TEM images of MNP-PLGA NPs with different loadings of OA-MNP are shown in Figure 1. OA-MNP had been successfully encapsulated into PLGA with 5% OA-MNP or less (Figure 1A, 1B and 1C) through hydrophobic interactions using the solid-in-oil-in-water solvent evaporation method. By contrast, the PLGA NPs loaded with 15% OA-MNP showed significant aggregation of MNP, which could be attributed to a higher loading amount and a stronger magnetic interaction between iron oxides (Figure 1D with insert). The MNP-PLGA NPs were nearly spherical with an average size of approximately 150 ± 20 nm. When the Tf concentration used was 1.0 mg/mL, the average size of Tf-modified PLGA NPs measured by DLS was approximately 464.6 nm with a polydispersity index of 0.057 (Figure 2D). This formulation will be used for *in vitro* studies. The zeta potentials were -28.07 ± 1.59 mV and -20.10 ± 1.26 mV for the MNP-PLGA and Tf-modified MNP-PLGA NPs, respectively. To study their stability, the changes in the zeta potentials of these NPs incubated in PBS (pH 7.2) were measured a few times over 96 h. The results indicated that the zeta potentials of MNP-PLGA NPs with and without Tf were stable, though there was a decrease after modification

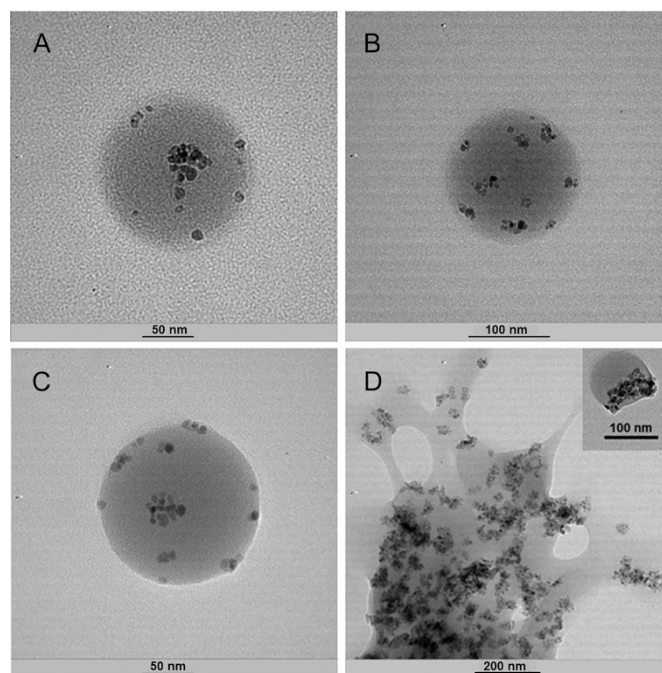


Figure 1. TEM images of MNP-PLGA NPs: (A) 1.5% OA-MNP-PLGA NPs, 2% PVA; (B) 5% OA-MNP-PLGA NPs, 2% PVA; (C) 5% OA-MNP-PLGA NPs, 4% PVA; (D) 15% OA-MNP-PLGA NPs, 2% PVA, inset: one representative photograph of the particle.

with Tf (data not shown).

Magnetic properties of MNP-PLGA NPs

To investigate the magnetic properties of MNP-PLGA NPs, magnetization measurements were made using a VSM. The curves in Figure 2A to 2C showed no remnant magnetic field and coercivity, indicating the presence of superparamagnetism in all the samples. The saturation magnetization (M_s) values of MNP, OA-MNP and MNP-PLGA NPs were 88.03, 81.99 and 10.85 emu/g, respectively (Figure 2A). The M_s value of as-synthesized Fe_3O_4 was 92 emu/g (95% of its bulk value), which might be due to its high specific surface area^[32]. Owing to the non-magnetic nature of OA and PLGA, the M_s values of OA-MNP and MNP-PLGA NPs were lower than that of MNP (Figure 2A). The M_s value of MNP-PLGA NPs increased with MNP loading in PLGA (Figure 2B). After MNP-PLGA NPs were modified with Tf, the M_s value (Figure 2C) was still higher than the reported value of 2 emu/g^[33].

TGA thermograms of MNP-PLGA NPs

Figure 3A shows the TGA thermograms of MNP, OA-MNP, MNP-PLGA NPs and Tf-modified MNP-PLGA NPs. The TGA thermogram of MNP showed approximately 2% weight loss from 20 to 700 $^\circ\text{C}$, possibly because of the loss of surface hydroxyl groups from the MNP. For OA-MNP, approximately 5.5% weight loss was observed in the first stage from 20 to 320 $^\circ\text{C}$ because of the loss of surface hydroxyl groups, while approximately 9% weight loss was observed in the sec-

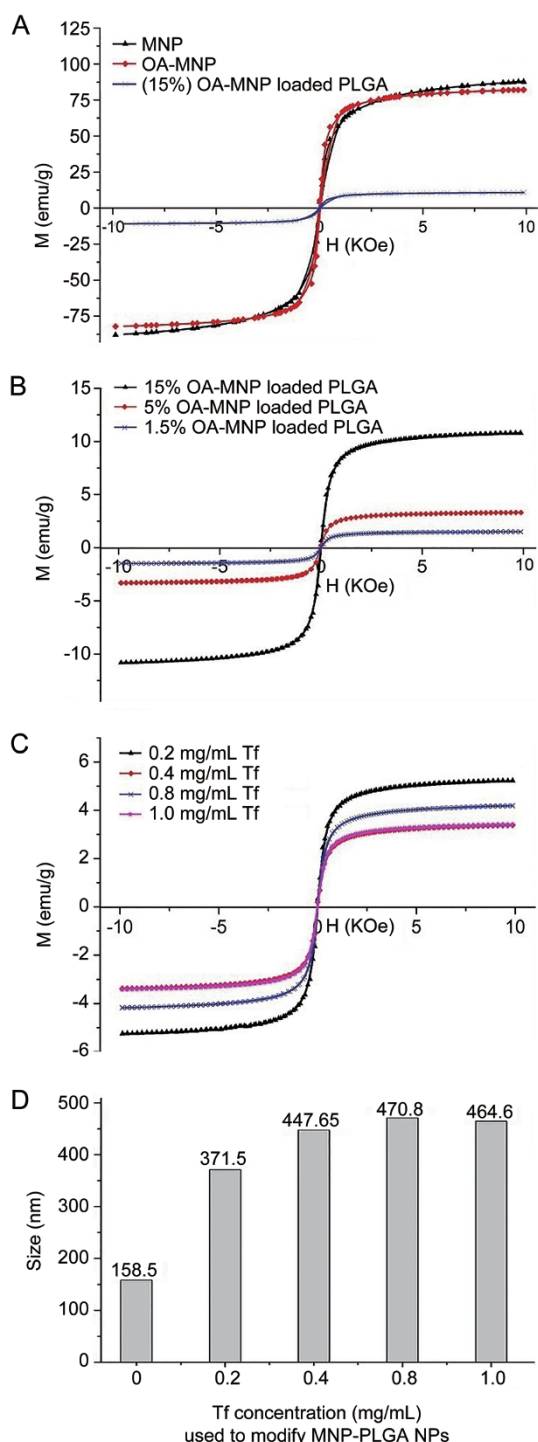


Figure 2. (A–C) Magnetization (M) curves measured under applied magnetic field (H) at 300 K, and (D) hydrodynamic diameter of Tf-modified MNP-PLGA NPs synthesized from increasing Tf concentration.

ond stage from 320 to 520 °C because of the removal of the OA monolayer from the OA-MNP. The weight loss profiles for MNP and OA-MNP were consistent with reported results^[27, 32]. The TGA thermogram of MNP-PLGA NPs showed approximately 94.3% weight loss from 250 to 400 °C, possibly because of the loss of surface hydroxyl groups and OA and to PLGA

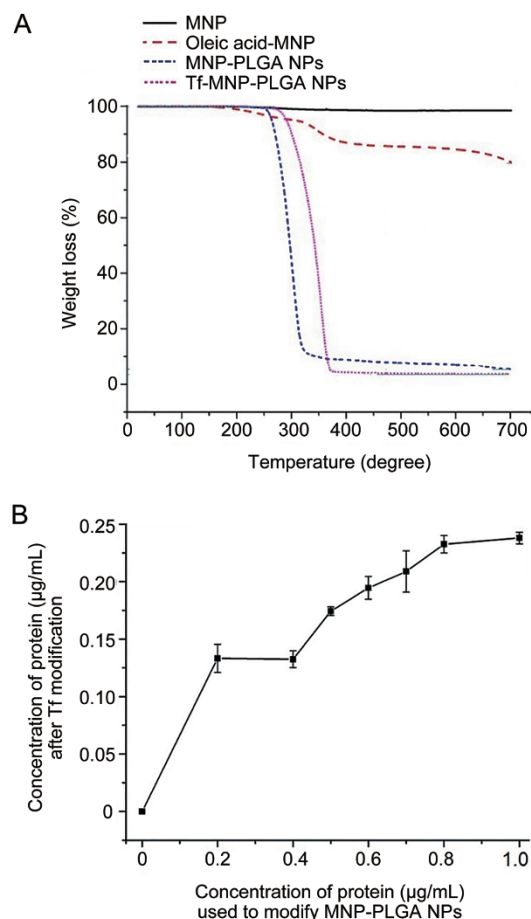


Figure 3. (A) TGA thermograms of MNP, OA-MNP, MNP-PLGA NPs and Tf-modified MNP-PLGA NPs, and (B) Surface concentration of adsorbed Tf on the surface of MNP-PLGA NPs with different concentrations of added Tf using BCA Protein Assay Kit.

degradation. Since a total of approximately 14.5% weight loss was observed for OA-MNP, the remaining 79.8% weight loss could arise from PLGA degradation. The TGA thermogram of Tf-modified MNP-PLGA NPs showed a weight loss of approximately 96.3%. The difference in weight loss between the MNP-PLGA NPs and Tf-modified MNP-PLGA NPs could be associated with the presence of Tf on the surface of the PLGA NPs.

The presence of Tf on the surface of PLGA NPs was determined using a BCA Protein Assay Kit (Figure 3B). Here, Tf solutions of various concentrations, ranging from 0 to 1.0 mg/mL, were prepared and used to modify MNP-PLGA NPs. Successful modification of PLGA NPs with Tf was apparent based on the increased absorbance reading for Tf-modified MNP-PLGA NPs prepared with increased Tf concentrations.

FTIR spectra of MNP-PLGA NPs

Figure 4 shows the FTIR spectra of MNP, OA-MNP and MNP-PLGA NPs. For MNP, the absorption band observed at 582 cm^{-1} may be attributed to Fe–O. The absorption band at 3412 cm^{-1} is the characteristic band for O–H vibrations and

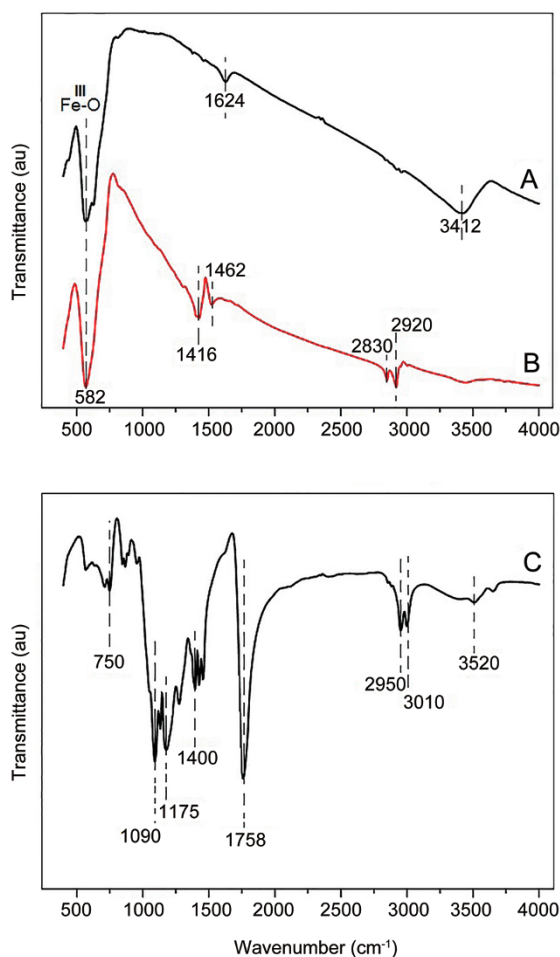


Figure 4. FTIR spectra of (A) MNP, (B) OA-MNP and (C) MNP-PLGA NPs.

indicates the presence of ferric hydroxide in the MNP. For OA-MNP, the absorption bands at 1416 and 1520 cm^{-1} are due to the symmetric and asymmetric stretching vibrations of $-\text{CH}_3$, respectively. The absorption bands at 2830 and 2920 cm^{-1} are due to the symmetric and asymmetric stretching vibrations of $-\text{CH}_2$, respectively. Owing to the interaction between PLGA and OA-MNP, the symmetric vibrations of $-\text{CH}$ for MNP-PLGA NPs were shifted to 2950 and 3010 cm^{-1} . These observations are consistent with reported results^[32].

Encapsulation efficiency and drug release

The encapsulation efficiency and drug release of PTX for MNP-PLGA NPs with and without Tf modification were studied (Table 1). Here, the Tf-modified PTX-MNP-PLGA NPs were synthesized with a Tf concentration of 1.0 mg/mL. The encapsulation efficiencies of PTX in MNP-PLGA NPs with and without Tf modification were 82.9% and 87.3%, respectively. The release profiles of PTX from MNP-PLGA NPs with and without Tf modification were observed to be similar (Figure 5). More than 80% of the drug was released within a period of 10 d. The release of PTX from PLGA NPs followed a biphasic profile, with a rapid drug release rate during the initial phase

Table 1. Encapsulation efficiency (EE) of PTX in different samples.

Samples	PTX-MNP-PLGA NPs	Tf-modified PTX-MNP-PLGA NPs
EE	87.3%	82.9%

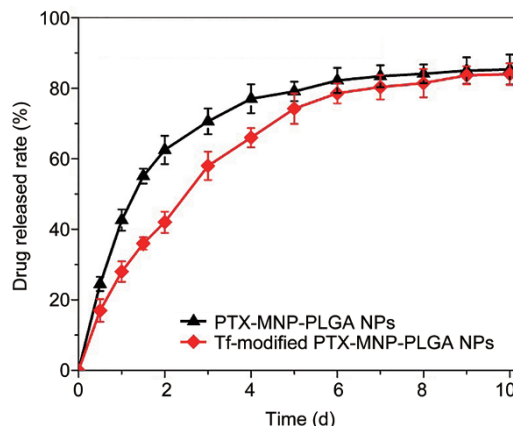


Figure 5. *In vitro* release profiles of PTX from PTX-MNP-PLGA NPs and Tf-modified PTX-MNP-PLGA NPs.

of incubation followed by a slow release.

In vitro cytotoxicity

The *in vitro* cytotoxicity of drug-loaded NPs in MCF-7 and U-87 cells was examined to determine their therapeutic efficiency (Figure 6). Here, PTX was selected as the model drug to evaluate the potential of Tf-modified MNP-PLGA NPs as a tumor-targeting nanocarrier for hydrophobic drugs^[34, 35]. For both MCF-7 and U-87 cells, the Tf-modified PTX-MNP-PLGA NPs showed the highest cytotoxicity effect, followed by Tf-modified NPs with free Tf, unmodified NPs and free PTX (Figure 6). Compared to the unmodified NPs, the Tf-modified PTX-MNP-PLGA NPs enhanced cellular uptake and increased cell cytotoxicity. However, in the presence of free Tf, the Tf-modified PTX-MNP-PLGA NPs showed a lower cytotoxicity effect. This may be attributed to the competition between Tf-modified PLGA NPs and free Tf for cellular uptake, which would in turn lower the cytotoxicity of Tf-modified PLGA NPs. Finally, the free PTX showed the lowest cytotoxicity effect relative to other NP formulations. In this case, the drug-resistant tumor cells could prevent intracellular accumulation of the free drug despite the high drug concentration used.

In vitro cellular uptake

The cellular uptake of drug-loaded NPs in MCF-7 and U-87 cells was examined by laser scanning confocal microscopy (Figure 7 and 8). To visualize the drug distribution within the cells, PTX was replaced by CM. Overall, CM was found mainly in the cytosol and around the nucleus, indicating that CM-MNP-PLGA NPs were successfully taken up by the cells. Cells treated with Tf-modified CM-MNP-PLGA NPs showed

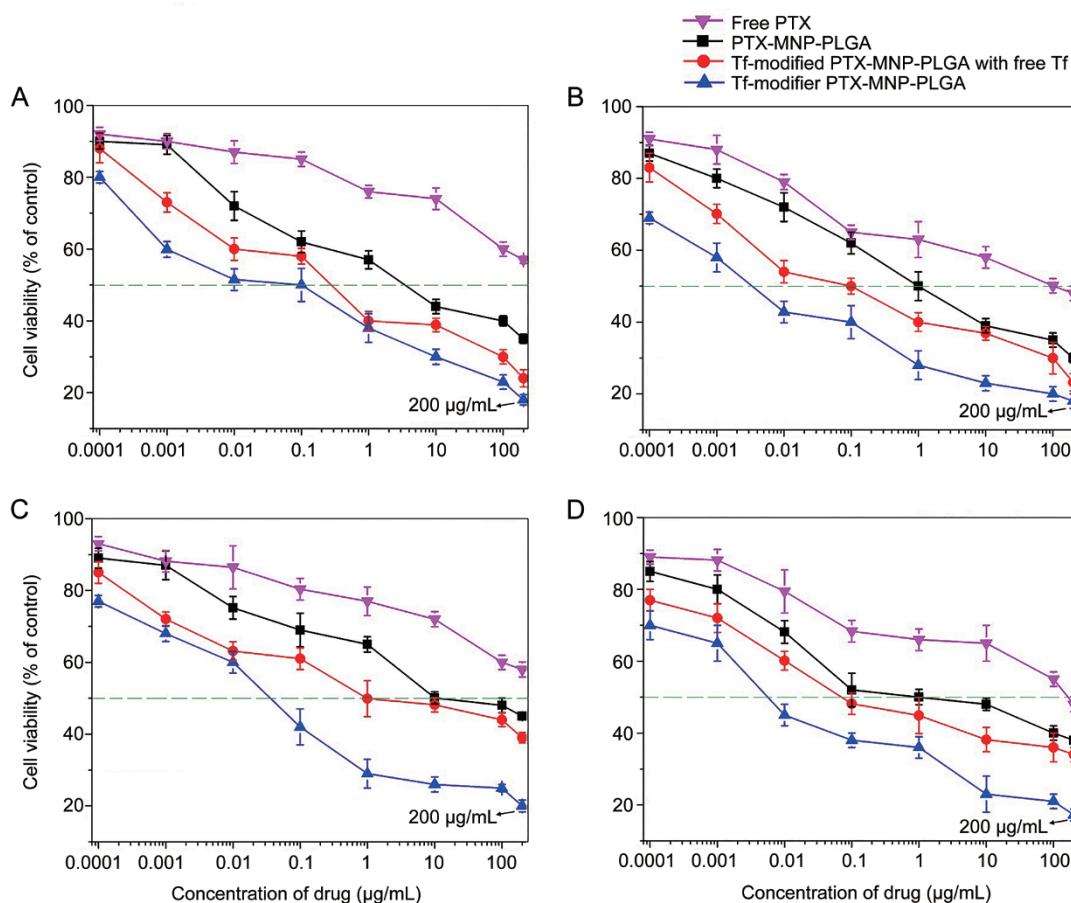


Figure 6. Viability of (A and B) MCF-7 and (C and D) U-87 cells after treatment with Tf-modified PTX-MNP-PLGA NPs, Tf-modified PTX-MNP-PLGA NPs with free Tf, PTX-MNP-PLGA NPs and free PTX for (A and C) 24 h and (B and D) 96 h.

greater fluorescence intensity than those treated with free Tf, unmodified NPs or free CM. Thus, Tf-modified NPs could lead to higher cellular uptake and hence greater drug accumulation. These confocal images are consistent with the cytotoxicity results reported earlier.

To support the qualitative analysis from the confocal images, the cellular uptake of drug-loaded NPs was quantified by measuring the percentage of drug internalized by the cells (Figure 9A and 9B). For both MCF-7 and U-87 cells, the uptake of CM or PTX was the highest for Tf-modified MNP-PLGA NPs, further verifying that the presence of Tf on the surface of PLGA NPs can trigger receptor-mediated endocytosis and result in enhanced intracellular delivery of drugs^[36]. The cellular uptake of drug-loaded NPs was also quantified in the presence of an applied magnetic field (Figure 9C). The cellular uptake efficiency of MNP-PLGA NPs seemed to be slightly greater in the presence of a magnetic field than in a non-magnetic condition; however, this effect did not reach statistical significance.

Discussion

Polymeric NPs modified with targeting ligands have attracted significant attention in the biomedical field because of their

ability to enhance intracellular delivery and provide sustained drug release^[37, 38]. Since the efficacy of chemotherapy is severely hindered by low drug accumulation in tumor cells, Tf-modified PLGA NPs that target the Tf receptors of tumors could improve the treatment of cancer. In this study, PTX (a potent antineoplastic agent) and MNP (for magnetic field-mediated delivery) were loaded into PLGA NPs via a solid-in-oil-in-water solvent evaporation process (Scheme 1A). Magnetically targeted nanodrug delivery systems have great potential for precise delivery of drugs under an applied magnetic field. Here, the MNP-PLGA NPs exhibited a superparamagnetic property (Figure 2A-2C), which was good enough to orient them to the target site and enhance the cellular uptake efficiency via an applied magnetic field. In other words, the Tf-modified magnetic PLGA NPs could have some advantages through their delivery of chemotherapeutics to the target location in the body and, consequently, reducing normal tissue toxicity.

To improve the stability of the system, amphiphilic PVA was added to stabilize the emulsified droplets by minimizing the coalescence and aggregation of newly formed NPs in the aqueous phase during the synthesis process. Moreover, amphiphilic PVA could enhance the encapsulation of MNP

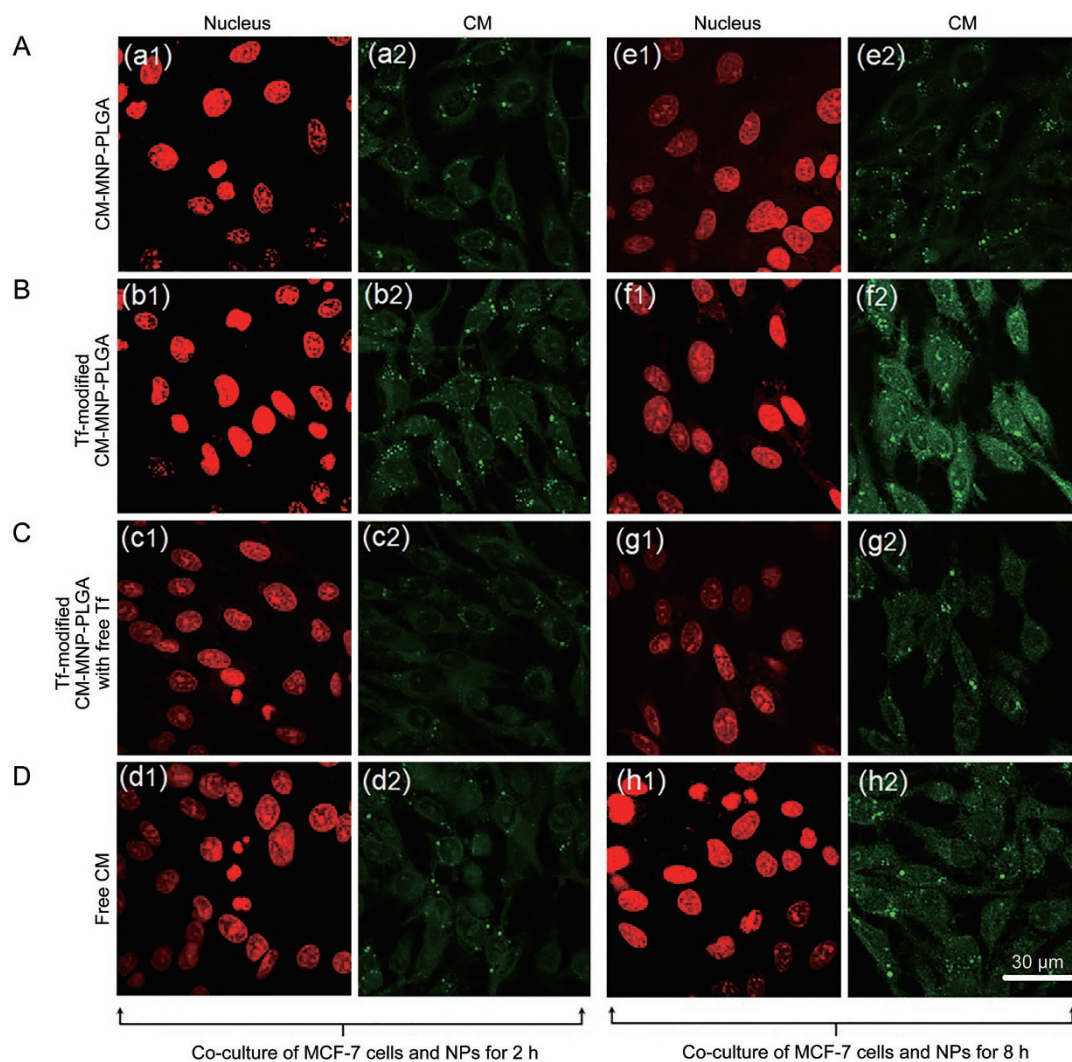


Figure 7. Confocal images depicting cellular uptake and drug distribution of (A) CM-MNP-PLGA NPs, (B) Tf-modified CM-MNP-PLGA NPs, (C) Tf-modified CM-MNP-PLGA NPs with free Tf, and (D) free CM in MCF-7 cells after (a–d) 2 h and (e–h) 8 h of incubation. The red shows the cell nuclei while the green shows the presence of CM.

into the polymeric nanoparticles via hydrophobic interactions. It has also been reported^[39, 40] that the concentration of PVA could influence the size of the NPs during preparation via the emulsion solvent evaporation method. However, as seen from TEM images, the NPs showed negligible particle size difference after using a high concentration [4% (*w/v*)] and a low concentration [2% (*w/v*)] of PVA solution (Figure 1). The surface of MNP-PLGA NPs was also modified with Tf via adsorption (Scheme 1B), and the presence of Tf was verified (Figure 3B). Surface modification of MNP-PLGA NPs with Tf did not significantly influence the encapsulation efficiency and drug release profile.

The effective cytotoxicity of Tf-modified MNP-PLGA NPs mainly depended on the amount of encapsulated chemotherapeutic drugs, the release behaviors of the encapsulated chemotherapeutic drugs and the cellular uptake efficiency. First, the Tf-modified MNP-PLGA NPs showed a similar encapsulation

efficiency for PTX as the unmodified NPs, which was helped to some extent by a high drug concentration. Second, the release of PTX from Tf-modified MNP-PLGA NPs exhibited a two-phase pattern: an initial rapid release in the first 4 d, followed by a relaxed slow release in the following days. The releasing property could depend on three dominating mechanisms: diffusion, swelling and degradation. Both the structure and size of the PLGA NPs could also impact the release profile. Third, drug-loaded NPs with Tf as the targeting ligand can enhance cellular uptake, provide greater internal drug release and promote a higher cytotoxicity effect (Scheme 1C)^[35, 41]. The results indicated that the Tf-modified PTX-MNP-PLGA NPs exhibited the highest cytotoxicity effect, followed by the Tf-modified NPs with free Tf, the unmodified NPs and the free PTX (Figure 6). The cellular uptake of drug-loaded NPs in MCF-7 and U-87 cells was examined by laser scanning confocal microscopy (Figure 7 and 8). The Tf-modified CM-

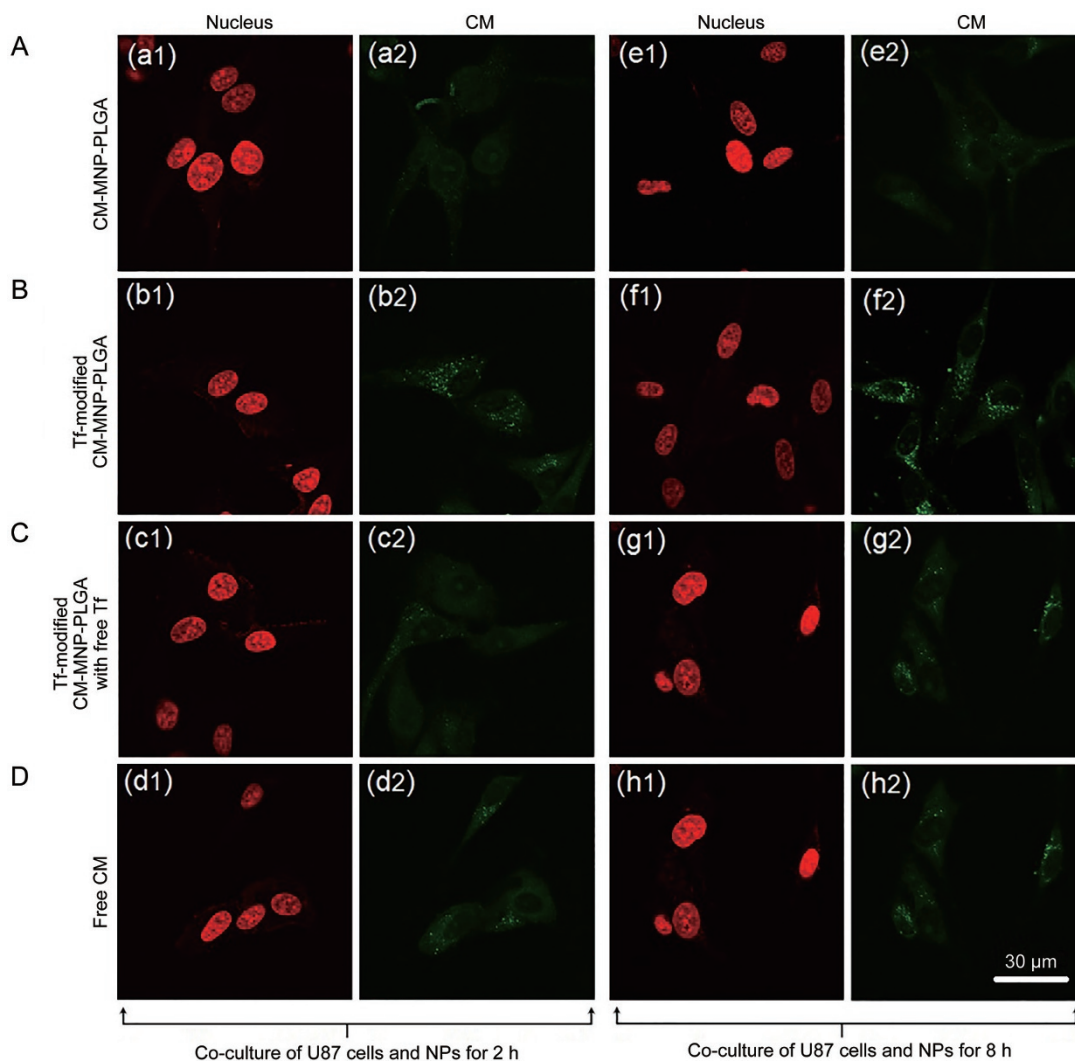


Figure 8. Confocal images depicting cellular uptake and drug distribution of (A) CM-MNP-PLGA NPs, (B) Tf-modified CM-MNP-PLGA NPs, (C) Tf-modified CM-MNP-PLGA NPs with free Tf, and (D) free CM in U-87 cells after (a–d) 2 h and (e–h) 8 h of incubation. The red shows the cell nuclei while the green shows the presence of CM.

MNP-PLGA NPs showed the highest intracellular accumulation, with most of the NPs clustering in the cytosol and around the nucleus. Additional consistent results were obtained by quantitative measurement of the percentage of drug internalized by the cells (Figure 9A and 9B). The cellular uptake efficiency of MNP-PLGA NPs seemed to be slightly greater in the presence of a magnetic field than in a non-magnetic condition; however, the difference was not statistically significant (Figure 9C). These Tf-targeting carriers could achieve higher cellular uptake efficiency, mainly because of their recognition of Tf receptors that are overexpressed in MCF-7 breast cancer and U-87 glioma cells^[42]. Moreover, Tf could surmount the drug resistance owing to membrane-associated drug resistance proteins such as P-glycoprotein^[43].

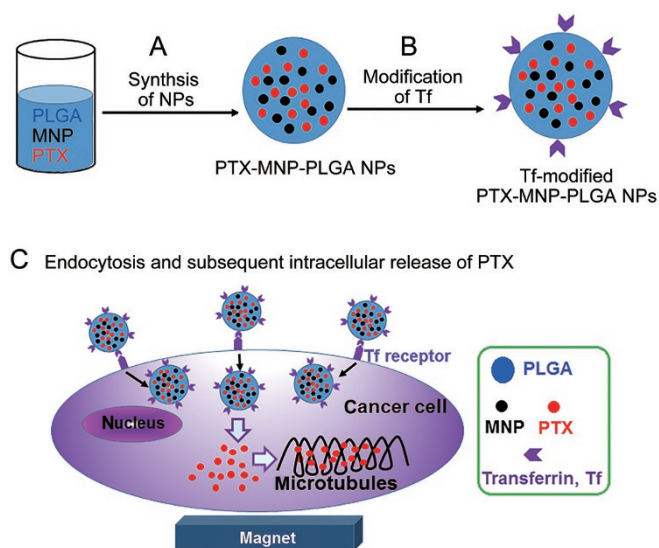
Conclusions

In this study, Tf-modified MNP-PLGA NPs were successfully

synthesized and characterized, and their cellular uptake efficiencies in MCF-7 breast cancer and U-87 glioma cells were demonstrated through receptor- and magnetic field-mediated delivery. Compared to unmodified NPs or free PTX, Tf-modified PTX-MNP-PLGA NPs demonstrated the highest cellular uptake efficiency and greatest antiproliferative effect on MCF-7 and U-87 cells. Overall, Tf-modified MNP-PLGA NPs are suitable drug carriers for the treatment of cancer.

Acknowledgements

The authors acknowledge the funding support from the National University of Singapore (NUS) (R279-000-357-275), the National Medical Research Council (NMRC, Singapore) (NMRC/EDG11may084), and the National Natural Science Foundation of China (81402885). Yan-na CUI also acknowledges the Chinese Scholarship Council for supporting her PhD program during her exchange at NUS.



Scheme 1. Synthesis of Tf-modified PTX-MNP-PLGA NPs via (A) solid-in-oil-in-water solvent evaporation process and (B) Tf adsorption on the surface of NPs. (C) Endocytosis of Tf-modified PTX-MNP-PLGA NPs and subsequent intracellular release of PTX.

Author contribution

Yan-na CUI performed the experiments, analyzed the data, prepared the figures and wrote the manuscript; Qing-xing XU and Pooya DAVOODI revised the manuscript and figures; De-ping WANG and Chi-Hwa WANG designed the study and supervised the team. The authors have read and approved the final version of the manuscript.

References

- Luan X, Guan YY, Lovell JF, Zhao M, Lu Q, Liu YR. Tumor priming using metronomic chemotherapy with neovasculature-targeted, nanoparticulate paclitaxel. *Biomaterials* 2016; 95: 60–73.
- Kareva I, Waxman DJ, Lakka Klement G. Metronomic chemotherapy: an attractive alternative to maximum tolerated dose therapy that can activate anti-tumor immunity and minimize therapeutic resistance. *Cancer Lett* 2015; 358: 100–6.
- Holmes FA, Walters RS, Theriault RL, Forman AD, Newton LK, Raber MN, et al. Phase II trial of taxol, an active drug in the treatment of metastatic breast cancer. *J Natl Cancer Inst* 1991; 83: 1797–805.
- McGuire WP, Rowinsky EK, Rosenshein NB, Grumbine FC, Ettinger DS, Armstrong DK, et al. Taxol: a unique antineoplastic agent with significant activity in advanced ovarian epithelial neoplasms. *Ann Intern Med* 1989; 111: 273–9.
- Rowinsky EK, Wright M, Monsarrat B, Lesser GJ, Donehower RC. Taxol: pharmacology, metabolism and clinical implications. *Cancer Surv* 1993; 17: 283–304.
- Cirstoiu-Hapca A, Buchegger F, Bossy L, Kosinski M, Gurny R, Delie F. Nanomedicines for active targeting: physico-chemical characterization of paclitaxel-loaded anti-HER2 immunonanoparticles and *in vitro* functional studies on target cells. *Eur J Pharm Sci* 2009; 38: 230–7.
- Zhang W, Shi Y, Chen Y, Ye J, Sha X, Fang X. Multifunctional Pluronic P123/F127 mixed polymeric micelles loaded with paclitaxel for the treatment of multidrug resistant tumors. *Biomaterials* 2011; 32: 2894–906.

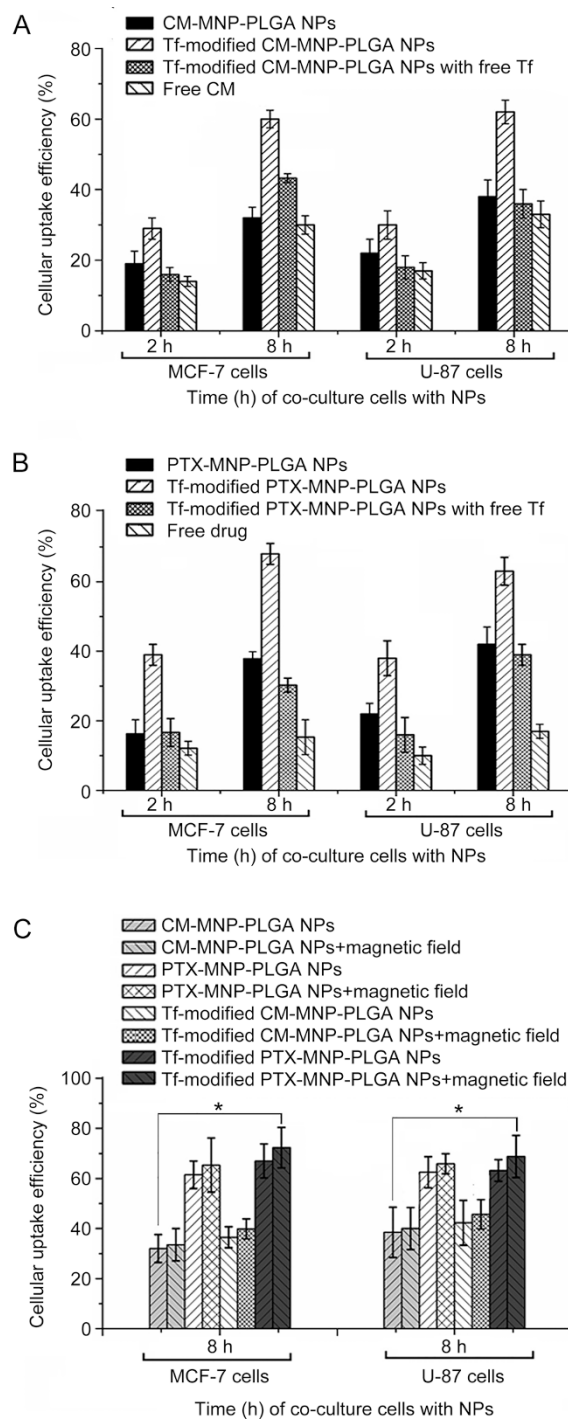


Figure 9. Cellular uptake efficiency of (A) CM-loaded PLGA NPs and (B) PTX-loaded PLGA NPs in MCF-7 and U-87 cells after 2 and 8 h of incubation in the absence of a magnetic field. (C) Comparison of cellular uptake efficiencies of drug-loaded PLGA NPs after 8 h of incubation in the presence of a magnetic field. * $P < 0.05$.

- Lee Y, Graeser R, Kratz F, Geckeler KE. Paclitaxel-loaded polymer nanoparticles for the reversal of multidrug resistance in breast cancer cells. *Adv Funct Mater* 2011; 21: 4211–8.
- Lehnert M. Clinical multidrug resistance in cancer: a multifactorial problem. *Eur J Cancer* 1996; 32A: 912–20.

- 10 Danhier F, Ansorena E, Silva JM, Coco R, Le Breton A, Préat V. PLGA-based nanoparticles: an overview of biomedical applications. *J Control Release* 2012; 161: 505–22.
- 11 Guo J, Gao X, Su L, Xia H, Gu G, Pang Z, *et al*. Aptamer-functionalized PEG-PLGA nanoparticles for enhanced anti-glioma drug delivery. *Biomaterials* 2011; 32: 8010–20.
- 12 Li J, Feng L, Fan L, Zha Y, Guo L, Zhang Q, *et al*. Targeting the brain with PEG-PLGA nanoparticles modified with phage-displayed peptides. *Biomaterials* 2011; 32: 4943–50.
- 13 Mahmoudi M, Simchi A, Imani M, Milani AS, Stroeve P. Optimal design and characterization of superparamagnetic iron oxide nanoparticles coated with polyvinyl alcohol for targeted delivery and imaging. *J Phys Chem B* 2008; 112: 14470–81.
- 14 Laurent S, Mahmoudi M. Superparamagnetic iron oxide nanoparticles: promises for diagnosis and treatment of cancer. *Int J Mol Epidemiol Genet* 2011; 2: 367–90.
- 15 Wahajuddin, Arora S. Superparamagnetic iron oxide nanoparticles: magnetic nanoplateforms as drug carriers. *Int J Nanomedicine* 2012; 7: 3445–71.
- 16 Polyak B, Friedman G. Magnetic targeting for site-specific drug delivery: applications and clinical potential. *Expert Opin Drug Deliv* 2009; 6: 53–70.
- 17 McCarron PA, Marouf WM, Donnelly RF, Scott C. Enhanced surface attachment of protein-type targeting ligands to poly(lactide-co-glycolide) nanoparticles using variable expression of polymeric acid functionality. *J Biomed Mater Res A* 2008; 87: 873–84.
- 18 Zhang N, Chittasupho C, Duangrat C, Siahaan TJ, Berkland C. PLGA nanoparticle-peptide conjugate effectively targets intercellular cell-adhesion molecule-1. *Bioconjug Chem* 2008; 19: 145–52.
- 19 Aravind A, Jeyamohan P, Nair R, Veerananarayanan S, Nagaoka Y, Yoshida Y, *et al*. AS1411 aptamer tagged PLGA-lecithin-PEG nanoparticles for tumor cell targeting and drug delivery. *Biotechnol Bioeng* 2012; 109: 2920–31.
- 20 Wu XL, Kim JH, Koo H, Bae SM, Shin H, Kim MS, *et al*. Tumor-targeting peptide conjugated pH-responsive micelles as a potential drug carrier for cancer therapy. *Bioconjug Chem* 2010; 21: 208–13.
- 21 Yue J, Liu S, Mo G, Wang R, Jing X. Active targeting and fluorescence-labeled micelles: preparation, characterization and cellular uptake evaluation. *J Control Release* 2011; 152: e258–60.
- 22 Zhang P, Hu L, Yin Q, Feng L, Li Y. Transferrin-modified c[RGDfK]-paclitaxel loaded hybrid micelle for sequential blood-brain barrier penetration and glioma targeting therapy. *Mol Pharm* 2012; 9: 1590–8.
- 23 Pang Z, Gao H, Yu Y, Guo L, Chen J, Pan S, *et al*. Enhanced intracellular delivery and chemotherapy for glioma rats by transferrin-conjugated biodegradable polymersomes loaded with doxorubicin. *Bioconjug Chem* 2011; 22: 1171–80.
- 24 Kuo YC, Lin PI, Wang CC. Targeting nevirapine delivery across human brain microvascular endothelial cells using transferrin-grafted poly(lactide-co-glycolide) nanoparticles. *Nanomedicine* 2011; 6: 1011–26.
- 25 Chang J, Paillard A, Passirani C, Morille M, Benoit JP, Betbeder D, *et al*. Transferrin adsorption onto PLGA nanoparticles governs their interaction with biological systems from blood circulation to brain cancer cells. *Pharm Res* 2012; 29: 1495–505.
- 26 Ramírez LP, Landfester K. Magnetic polystyrene nanoparticles with a high magnetite content obtained by miniemulsion processes. *Macromol Chem Phys* 2003; 204: 22–31.
- 27 Jain TK, Morales MA, Sahoo SK, Leslie-Pelecky DL, Labhasetwar V. Iron oxide nanoparticles for sustained delivery of anticancer agents. *Mol Pharm* 2005; 2: 194–205.
- 28 Liu X, Kaminski MD, Chen H, Torno M, Taylor L, Rosengart AJ. Synthesis and characterization of highly-magnetic biodegradable poly(D,L-lactide-co-glycolide) nanospheres. *J Control Release* 2007; 119: 52–8.
- 29 Chang J, Jallouli Y, Kroubi M, Yuan XB, Feng W, Kang CS, *et al*. Characterization of endocytosis of transferrin-coated PLGA nanoparticles by the blood-brain barrier. *Int J Pharm* 2009; 379: 285–92.
- 30 Gan CW, Feng SS. Transferrin-conjugated nanoparticles of poly(lactide)-D-alpha-tocopheryl polyethylene glycol succinate diblock copolymer for targeted drug delivery across the blood-brain barrier. *Biomaterials* 2010; 31: 7748–57.
- 31 Banquy X, Suarez F, Argaw A, Rabanel JM, Grutter P, Bouchard JF, *et al*. Effect of mechanical properties of hydrogel nanoparticles on macrophage cell uptake. *Soft Matter* 2009; 5: 3984–91.
- 32 Anandhariya N, Chudasama B, Mehta RV, Upadhyay RV. Biodegradable thermoresponsive polymeric magnetic nanoparticles: a new drug delivery platform for doxorubicin. *J Nanopart Res* 2011; 13: 1677–88.
- 33 Liu Q, Zhang J, Xia W, Gu H. Magnetic field enhanced cell uptake efficiency of magnetic silica mesoporous nanoparticles. *Nanoscale* 2012; 4: 3415–21.
- 34 Scripture CD, Figg WD, Sparreboom A. Paclitaxel chemotherapy: from empiricism to a mechanism-based formulation strategy. *Ther Clin Risk Manag* 2005; 1: 107–14.
- 35 Zhang P, Hu L, Yin Q, Zhang Z, Feng L, Li Y. Transferrin-conjugated polyphosphoester hybrid micelle loading paclitaxel for brain-targeting delivery: synthesis, preparation and *in vivo* evaluation. *J Control Release* 2012; 159: 429–34.
- 36 Li SD, Huang L. Pharmacokinetics and biodistribution of nanoparticles. *Mol Pharm* 2008; 5: 496–504.
- 37 Li Y, He H, Jia X, Lu WL, Lou J, Wei Y. A dual-targeting nanocarrier based on poly(amidoamine) dendrimers conjugated with transferrin and tamoxifen for treating brain gliomas. *Biomaterials* 2012; 33: 3899–908.
- 38 Xin H, Sha X, Jiang X, Zhang W, Chen L, Fang X. Anti-glioblastoma efficacy and safety of paclitaxel-loading Angiopep-conjugated dual targeting PEG-PCL nanoparticles. *Biomaterials* 2012; 33: 8167–76.
- 39 Guo H, Yang D, Yang M, Gao Y, Liu Y, Li H. Dual responsive pickering emulsions stabilized by constructed core crosslinked polymer nanoparticles via reversible covalent bonds. *Soft Matter* 2016; 12: 9683–91.
- 40 Bohrey S, Chourasiya V, Pandey A. Polymeric nanoparticles containing diazepam: preparation, optimization, characterization, *in-vitro* drug release and release kinetic study. *Nano Conver* 2016; 3: 3.
- 41 Sahoo SK, Labhasetwar V. Enhanced antiproliferative activity of transferrin-conjugated paclitaxel-loaded nanoparticles is mediated via sustained intracellular drug retention. *Mol Pharm* 2005; 2: 373–83.
- 42 Lu C, Xing MMQ, Zhong W. Shell cross-linked and hepatocyte-targeting nanoparticles containing doxorubicin via acid-cleavable linkage. *Nanomedicine* 2011; 7: 80–7.
- 43 Wang F, Jiang X, Yang DC, Elliott RL, Head JF. Doxorubicin-gallium-transferrin conjugate overcomes multidrug resistance: evidence for drug accumulation in the nucleus of drug resistant MCF-7/ADR cells. *Anticancer Res* 2000; 20: 799–808.